

Primordial black holes ensued from exponential potential and coupling parameter in nonminimal derivative inflation model

Soma Heydari^a and Kayoomars Karami^b

*Department of Physics, University of Kurdistan,
Pasdaran Street, P.O. Box 66177-15175, Sanandaj, Iran*

(Dated: March 17, 2022)

Abstract

Here, Primordial Black Holes (PBHs) creation from exponential potential has been inquired, through gravitationally raised friction emanated from the nonminimal coupling between gravity and field derivative setup. Setting a two-parted exponential function of inflaton field as coupling parameter, and fine-tuning of four parameter Cases of our model, we could sufficiently slow down the inflaton owing to high friction during an ultra slow-roll phase. This empowers us to achieve enough enhancement in the amplitude of curvature perturbations power spectra, via numerical solving of Mukhanov-Sasaki equation. Thereafter, we illustrate the generation of four PBHs with disparate masses in RD era, corresponding to our four parameter Cases. Two specimens of these PBHs with stellar $\mathcal{O}(10)M_{\odot}$ and earth $\mathcal{O}(10^{-6})M_{\odot}$ masses can be appropriate to explicate the LIGO-VIRGO events, and the ultrashort-timescale microlensing events in OGLE data, respectively. Another two Cases of PBHs have asteroid masses around $\mathcal{O}(10^{-13})M_{\odot}$ and $\mathcal{O}(10^{-15})M_{\odot}$ with abundance of 96% and 95% of the Dark Matter (DM) content of the universe. Furthermore, we scrutinize the induced Gravitational Waves (GWs) ensued from PBHs production in our model. Subsequently, we elucidate that their contemporary density parameter spectra (Ω_{GW_0}) for all predicted Cases have acmes which lie in the sensitivity scopes of the GWs detectors, thereupon the verity of our conclusions can be verified in view of deduced data from these detectors. At length, our numerical outcomes exhibit a power-law behavior for the spectra of Ω_{GW_0} with respect to frequency as $\Omega_{\text{GW}_0}(f) \sim (f/f_c)^n$ in the proximity of acmes position. As well, in the infrared regime $f \ll f_c$, the log-reliant form of power index as $n = 3 - 2/\ln(f_c/f)$ is attained.

^a s.heydari@uok.ac.ir

^b kkarami@uok.ac.ir

I. INTRODUCTION

It is known that, enough sizable amplitude of curvature perturbations in the inflationary epoch could give rise to form the ultra-condensed districts of the primal cosmos, thence gravitationally collapse of these sectors terminate in generation of Primordial Black Holes (PBHs) in the Radiation Dominated (RD) era. The first intimation of this outline should be addressed to the researches [1–4].

The enigmatic nature of Dark Matter (DM) [5], and unsuccessful observation of particle DM, beside the latest thriving revelation of Gravitational Waves (GWs) emerged from the coalescence of two black holes with masses around $30M_{\odot}$ (M_{\odot} signifies the solar mass) by LIGO-Virgo Collaboration [6–10], have widely inspired the researchers to contemplate PBHs as interesting source for the entire or a percentage of the universe DM content and GWs [11–63]. By reason of the non-stellar inception of PBHs generation, their masses are not confined to Chandrasekhar restriction and they could place in the vast range of masses. PBHs at the mass scope of $\mathcal{O}(10^{-5})M_{\odot}$ with the fractional exuberance around $\mathcal{O}(10^{-2})$, can be regarded as the genesis of ultrashort-timescale microlensing events in the OGLE data, because of settling in the sanctioned area by OGLE data [36]. Furthermore PBHs within the scope of asteroid masses $\mathcal{O}(10^{-16} - 10^{-11})M_{\odot}$ can comprise all DM content of the universe [21–23, 37–39, 56, 57, 60], inasmuch as the gravitational femtolensing of gamma-ray bursts [64] is inoperative by way of weakening the lensing effects via the wave effects [37, 38], and Subaru Hyper Supreme-Cam (Subaru HSC) microlensing observations decree no constraint on PBHs in the mass ranges lower than $10^{-11}M_{\odot}$. Moreover, the imposed constraint by white dwarf [65] has been shown to be ineffective using numerical simulations in [66].

It is well understood that, so as to generate detectable PBHs in RD stage, the amplitude of primordial curvature perturbations (\mathcal{R}) must be amplified to specific order during inflationary era. Recrudescence of superhorizon scales related to enhanced amplitude of \mathcal{R} to the horizon in RD domain, gives rise to formation of ultradense zones, and PBHs can be produced from gravitationally collapse of these zones. A sufficient amplification of the power spectrum of \mathcal{R} to order $\mathcal{P}_{\mathcal{R}} \sim \mathcal{O}(10^{-2})$ at small scales is necessitated to generate detectable PBHs, whereas the recent observations of CMB anisotropies confined the power spectrum of \mathcal{R} to $\mathcal{P}_{\mathcal{R}}^* \sim 2.1 \times 10^{-9}$ [67] at pivot scale $k_* = 0.05 \text{ Mpc}^{-1}$. Heretofore, multifarious technical methods have been suggested by researchers to achieve amplified curvature power

spectrum with the amount around 10^7 times larger than scalar power spectrum at CMB scales [11–63]. Pi *et al.* in [61] could attain this amplification in $\mathcal{P}_{\mathcal{R}}$ using the Starobinsky R^2 model with a non-minimally coupled scalar field χ , through the mortal oscillations during the transition from the first phase of inflation to the second one. Recently, a similar model of two-field inflation has been proposed by Braglia *et al.* for generating PBHs and GWs [48]. In the model unlike that of Pi *et al.* [49] a very broad peak in the Scalar power spectrum and therefore PBHs with a broader mass function, and also specific oscillatory pattern in the stochastic gravitational wave background, akin to [64], could have been produced. Further similar model for producing oscillatory GWs is presented in [50]. Another method to amplify $\mathcal{P}_{\mathcal{R}}$ is proposed by [44, 45, 51–53, 62, 63] through applying inflationary potentials for their models with an inflection point. In these models an enhancement in the scalar power spectrum is attained by slowing down the inflaton field during a transient era of Ultra Slow-Roll (USR) inflation in comparison with Slow-Roll inflation because of an inflection point in the potential. Another appropriate way to produce an USR phase and slowing down the inflaton is increasing the friction by applying the NonMinimal Derivative Coupling to gravity (NMDC) framework for the models [55–59, 68–72].

The framework of NMDC constructed of nonminimal coupling between field derivative and the Einstein tensor is a subdivision of the comprehensive scalar-tensor theories with second order equation of motion, like as General Relativity (GR), to wit the Horndeski theory [69–73]. The Horndeski theory forestalls the model from negative energy and the Ostrogradski instability [74–77].

It is known that, exponential potential drives an endless inflationary epoch in standard model of inflation [78]. Moreover, as regards the inconsistency of the exponential potential in the standard framework with Planck 2018 TT,TE,EE+lowE+lensing+BK14+BAO data at CMB scale [67, 78], we try to reclaim this potential in NMDC setup. In other words the feature of gravitationally enhanced friction in NMDC setup inspires us to evaluate the compatibility of exponential form of potential in this framework with the latest Planck’s observational data on large scales, and furthermore examine the likelihood of PBHs generation in detectable mass scopes at small scales contemporaneously. In [55] the production of PBHs in transient NMDC framework with a power-law potential $V(\phi) \propto \phi^{2/5}$ has been investigated by Fu *et al.* but in their work the NMDC term just operate within the USR epoch and dose not have an indelible impression due to the selected form of coupling pa-

parameter between field derivative and gravity. In the present work, we have selected a special exponential form of two-parted coupling function so as to have the NMDC framework all over the inflationary era.

Dissemination of produced secondary gravitational waves coeval with PBHs generation, could be the further upshot of reverting the enhanced amplitude of primordial scalar perturbations to the horizon in RD era [21–23, 27, 28, 52, 56, 57, 62, 63, 79–95]. In this article, we compute the present density parameter spectra of induced GWs as a supplementary effect of PBHs generation in NMDC framework, and peruse the verity of our numerical outcomes in comparison with the sensitivity scopes of multifarious GWs detectors. At length we appraise the inclination of the energy spectra of GWs in disparate ranges of frequency.

This paper is classified as follows. In Sec. II, we review succinctly the foundation of nonminimal derivative coupling structure. The Sec. III, is given over to clarifying the appropriate technique to amplify the amplitude of the curvature power spectrum at small scale to order $\mathcal{O}(10^{-2})$ in NMDC model. Thence, we investigate the feasibility of PBHs generation with varietal masses and fractional abundances in Sec. IV, and present energy spectra of induced GWs in our setup are computed in Sec. V. After all, the foreshortened outcomes are enumerated in Sec. VI.

II. NONMINIMAL DERIVATIVE COUPLING FRAMEWORK

The NonMinimal Derivative Coupling (NMDC) model is depicted by the generic action [68–72] as

$$S = \int d^4x \sqrt{-g} \left[\frac{1}{2}R - \frac{1}{2}(g^{\mu\nu} - \xi G^{\mu\nu}) \partial_\mu \phi \partial_\nu \phi - V(\phi) \right], \quad (1)$$

wherein the derivative of inflaton field is coupled to the Einstein tensor via the coupling parameter denoted by ξ with dimension of $(\text{mass})^{-2}$, and g is determinant of the metric tensor $g_{\mu\nu}$, R is the Ricci scalar, $G^{\mu\nu}$ is the Einstein tensor, and $V(\phi)$ signifies the potential of the scalar field ϕ . Referring to our erstwhile explanation, this action (1) pertains to general scalar-tensor theories viz the Horndeski theory with the second order equations of motion. The general Lagrangian of this theories embodies the expression $G_5(\phi, X)G^{\mu\nu}(\nabla_\mu \nabla_\nu \phi)$, wherein G_5 is a generic function of ϕ and kinetic term $X = -\frac{1}{2}g^{\mu\nu} \partial_\mu \phi \partial_\nu \phi$. Presuming $G_5 = -\Theta(\phi)/2$, and $\xi \equiv d\Theta/d\phi$, thereafter integrating partially, the NMDC action (1) is retrieved from the Horndeski Lagrangian. The coupling parameter ξ can be considered as a

constant parameter [68–72], or as a function of ϕ [56, 57, 59, 96].

With this in mind, we excogitate $\xi = \theta(\phi)$ as an exponential two-parted function of ϕ , so as to not only ameliorate the observational prognostications of the exponential potential on large scales, but also generation of PBHs and induced GWs on small scales could be expounded prosperously in NMDC setup. At first we initiate to study the dynamics of homogeneous and isotropic background having the flat Friedmann-Robertson-Walker (FRW) metric as $g_{\mu\nu} = \text{diag}(-1, a^2(t), a^2(t), a^2(t))$, in which $a(t)$ and t denote the scale factor and cosmic time. Thenceforth, we reconsider the attained equations for propagated perturbations during inflation era in NMDC model depicted through action (1).

The Friedmann equations and the equation of motion governing the scalar field ϕ ensued from taking derivative of action (1) with regard to $g_{\mu\nu}$ and ϕ can be obtained as following form

$$3H^2 - \frac{1}{2}\left(1 + 9H^2\theta(\phi)\right)\dot{\phi}^2 - V(\phi) = 0, \quad (2)$$

$$2\dot{H} + \left(-\theta(\phi)\dot{H} + 3\theta(\phi)H^2 + 1\right)\dot{\phi}^2 - H\theta_{,\phi}\dot{\phi}^3 - 2H\theta(\phi)\dot{\phi}\ddot{\phi} = 0, \quad (3)$$

$$(1 + 3\theta(\phi)H^2)\ddot{\phi} + \left(1 + \theta(\phi)(2\dot{H} + 3H^2)\right)3H\dot{\phi} + \frac{3}{2}\theta_{,\phi}H^2\dot{\phi}^2 + V_{,\phi} = 0, \quad (4)$$

where $H \equiv \dot{a}/a$ signifies the Hubble parameter, the dot symbol implies derivative with regard to the cosmic time t , and $(, \phi)$ denotes derivative with regard to ϕ . We also stipulate that the reduced Planck mass equates with one ($M_P = 1/\sqrt{8\pi G} = 1$), all over this article. Pursuant the calculations of [69, 70] in NMDC framework, slow-roll parameters are acquainted as follows

$$\varepsilon \equiv -\frac{\dot{H}}{H^2}, \quad \delta_\phi \equiv \frac{\ddot{\phi}}{H\dot{\phi}}, \quad \delta_X \equiv \frac{\dot{\phi}^2}{2H^2}, \quad \delta_D \equiv \frac{\theta(\phi)\dot{\phi}^2}{4}. \quad (5)$$

The slow-roll approximation of inflation is validated provided that $\{\epsilon, |\delta_\phi|, \delta_X, \delta_D\} \ll 1$, and thereunder the potential energy term of energy density is prevailing owing to negligibility of kinetic energy term. Thus the equations (2)-(4) can be recast as the following abridged form

$$3H^2 \simeq V(\phi), \quad (6)$$

$$2\dot{H} + \mathcal{A}\dot{\phi}^2 - H\theta_{,\phi}\dot{\phi}^3 \simeq 0, \quad (7)$$

$$3H\dot{\phi}\mathcal{A} + \frac{3}{2}\theta_{,\phi}H^2\dot{\phi}^2 + V_{,\phi} \simeq 0, \quad (8)$$

in which

$$\mathcal{A} \equiv 1 + 3\theta(\phi)H^2. \quad (9)$$

On the presumption that the following condition

$$|\theta_{,\phi}H\dot{\phi}| \ll \mathcal{A}, \quad (10)$$

is confirmed during slow-roll epoch, the equations (6)-(8) can be simplified as

$$3H^2 \simeq V(\phi), \quad (11)$$

$$2\dot{H} + \mathcal{A}\dot{\phi}^2 \simeq 0, \quad (12)$$

$$3H\dot{\phi}\mathcal{A} + V_{,\phi} \simeq 0. \quad (13)$$

Utilizing equations (11) and (13), the first slow-roll parameter can be written as

$$\varepsilon \simeq \delta_X + 6\delta_D \simeq \frac{\varepsilon_V}{\mathcal{A}}, \quad (14)$$

in which

$$\varepsilon_V \equiv \frac{1}{2} \left(\frac{V_{,\phi}}{V} \right)^2. \quad (15)$$

It is clear from (14) that, $\mathcal{A} \simeq 1$ leads to $\varepsilon \simeq \varepsilon_V$, and the standard model of slow-roll inflation is retrieved. Furthermore, $\mathcal{A} \gg 1$ gives rise to $\varepsilon \ll \varepsilon_V$ and considerable increment in the friction, and as a consequence more slowing down the inflaton field during USR phase with regard the slow-roll outlook. Severe lessening of the velocity of inflaton field in USR domain due to enlarged friction results in acute reduction of the first slow-roll parameter and thence remarkable increment in the scalar power spectrum. Hereupon, we ponder the power spectrum of \mathcal{R} in NMDC setup at the instant of Hubble horizon traversing via comoving wavenumber k [71] as follows

$$\mathcal{P}_{\mathcal{R}} = \frac{H^2}{8\pi^2 Q_s c_s^3} \Big|_{c_s k = aH}, \quad (16)$$

where, in accordance with computations of [70], we have

$$Q_s = \frac{w_1(4w_1w_3 + 9w_2^2)}{3w_2^2}, \quad (17)$$

$$c_s^2 = \frac{3(2w_1^2w_2H - w_2^2w_4 + 4w_1\dot{w}_1w_2 - 2w_1^2\dot{w}_2)}{w_1(4w_1w_3 + 9w_2^2)}, \quad (18)$$

and

$$w_1 = 1 - 2\delta_D, \quad (19)$$

$$w_2 = 2H(1 - 6\delta_D), \quad (20)$$

$$w_3 = -3H^2(3 - \delta_X - 36\delta_D), \quad (21)$$

$$w_4 = 1 + 2\delta_D. \quad (22)$$

Utilizing equations (11)-(13) associated with the background evolution under the slow-roll approximation, the scalar power spectrum (16) takes the following form

$$\mathcal{P}_{\mathcal{R}} \simeq \frac{V^3}{12\pi^2 V_{,\phi}^2} \mathcal{A} \simeq \frac{V^3}{12\pi^2 V_{,\phi}^2} \left(1 + \theta(\phi)V\right). \quad (23)$$

The observational restriction on amplitude of the scalar power spectrum is quantified by Planck collaboration from the anisotropies of cosmic microwave background (CMB) at pivot scale ($k_* = 0.05 \text{ Mpc}^{-1}$) [67] as

$$\mathcal{P}_{\mathcal{R}}(k_*) \simeq 2.1 \times 10^{-9}. \quad (24)$$

The association of scalar spectral index n_s with the slow-roll parameters in the NMDC model can be computed from the curvature power spectrum through the definition $n_s - 1 \equiv d \ln \mathcal{P}_{\mathcal{R}} / d \ln k$ [56] as follows

$$n_s \simeq 1 - \frac{1}{\mathcal{A}} \left[6\varepsilon_V - 2\eta_V + 2\varepsilon_V \left(1 - \frac{1}{\mathcal{A}}\right) \left(1 + \frac{\theta_{,\phi}}{\theta(\phi)} \frac{V(\phi)}{V_{,\phi}}\right) \right], \quad (25)$$

in which

$$\eta_V = \frac{V_{,\phi\phi}}{V}. \quad (26)$$

In the case of $\theta(\phi) = 0$ the coupling parameter is faded away and standard slow-roll inflationary formalism is retrieved. The tensor power spectrum at $c_t k = aH$ and the tensor-to-scalar ratio in NMDC framework under slow-roll approximation have been computed in [71] as the following form

$$\mathcal{P}_t = \frac{2H^2}{\pi^2}, \quad (27)$$

$$r \simeq 16\varepsilon \simeq 16 \frac{\varepsilon_V}{\mathcal{A}}. \quad (28)$$

The observational constraint on the scalar spectral index n_s in accordance with Planck 2018 TT,TE,EE+lowE+lensing+BK14 +BAO data at the 68% CL , and the upper limit on the

tensor-to-scalar ratio r at 95% CL [67] are as follows

$$n_s = 0.9670 \pm 0.0037, \quad (29)$$

$$r < 0.065. \quad (30)$$

III. AMPLIFICATION OF CURVATURE POWER SPECTRUM

It is corroborated that, generation of observable PBHs and GWs originates from remarkable enhancement in the amplitude of curvature power spectrum during transient USR phase on small scales. In NMDC framework the appropriate model parameters and coupling function between field derivative and the Einstein tensor should be elected so as to enhance the friction during USR era [55–59]. In pursuance of this objective we delineate two-parted exponential form of coupling function $\theta(\phi)$ so as to have a NMDC model with prognostications in conformity with the latest observational data on large scales (CMB) as well a generated peak in the scalar power spectrum on smaller scales, as follows

$$\theta(\phi) = \theta_I(\phi) \left(1 + \theta_{II}(\phi) \right), \quad (31)$$

in which

$$\theta_I(\phi) = \frac{e^{\alpha\phi}}{M^2}, \quad (32)$$

$$\theta_{II}(\phi) = \frac{\omega}{\sqrt{\left(\frac{\phi-\phi_c}{\sigma}\right)^2 + 1}}. \quad (33)$$

The first portion of our coupling function (32) is a generic exponential form of the taken coupling parameters by [69–71, 96]. Another portion (33) is given by Fu et al. [55] so as to inspect the possibility of PBHs and GWs generation in a transient NMDC framework for the potential $V(\phi) \propto \phi^{2/5}$, however we combine these two functions by way of (31). Apropos of $\theta_{II}(\phi)$, this function has an acme at crucial value of field $\phi = \phi_c$ with the height and width denoted by ω and σ . It can be inferred from (33) that, for farther field values from the crucial value ϕ_c the function $\theta_{II}(\phi)$ melts away and our general coupling function (31) is dominated by its first term (32). The presentment of exponential function $\theta_I(\phi)$ is necessitated in pursuance of rectifying prognostications of our model on the CMB scales with the recent observational data. Furthermore, $\theta_I(\phi)\theta_{II}(\phi)$ beside fine tuning of model parameters are productive of increase in the amplitude of curvature power spectrum on

TABLE I. Tuned parameters for the Cases A, B, C, and D. Also ΔN denotes the duration of viable inflationary epoch for each Case. The parameter λ is specified by the power spectrum constraint (24) at horizon traversing e -fold number (N_*).

| # | ω | σ | ϕ_c | λ | ΔN |
|--------|---------------------|------------------------|----------|------------------------|------------|
| Case A | 3.869×10^7 | 1.53×10^{-11} | 0.1272 | 3.68×10^{-10} | 53 |
| Case B | 3.879×10^7 | 1.67×10^{-11} | 0.125 | 3.71×10^{-10} | 58 |
| Case C | 5.146×10^7 | 1.86×10^{-11} | 0.117 | 3.68×10^{-10} | 60 |
| Case D | 5.761×10^7 | 2.17×10^{-11} | 0.112 | 3.63×10^{-10} | 60 |

small scales to sufficient value to produce the observable PBHs and GWs. Concerning the portions of coupling function (32)-(33), parameters $\{\alpha, \omega\}$ are dimensionless whereas the parameters $\{\phi_c, \sigma, M\}$ have dimensions of mass. Inasmuch as, in standard framework of inflation the exponential potential drives an endless inflationary epoch [78] and, as regards the inconsistency of the prognostications of this form of potential at CMB scales in view of Planck 2018 TT,TE,EE+lowE+lensing+BK14+BAO data [67, 78], we try to amend the results of this potential in NMDC framework. Ergo, in the following we pursue the objective if the exponential potential could derive the viable inflation on large scale contemporaneous with production detectable PBHs and GWs on smaller scales in NMDC framework. The exponential potential is given as follows

$$V(\phi) = \lambda e^{k\phi}, \quad (34)$$

where k is dimensionless parameter, and λ can be fixed through the constraint of scalar power spectrum at pivot scale k_* (24) in our setup.

In this stage we ponder over the estimation of the order of required multiplication factor to increase the amplitude of the scalar power spectrum $\mathcal{P}_{\mathcal{R}}$ on small scales to order $\mathcal{O}(10^{-2})$

TABLE II. Computed numerical upshots for Cases of Table I. The quantities $\mathcal{P}_{\mathcal{R}}^{\text{peak}}$, $f_{\text{PBH}}^{\text{peak}}$, and $M_{\text{PBH}}^{\text{peak}}$ denote the values of the scalar power spectrum, fractional abundance of PBHs, and the PBH mass at acme position $\phi = \phi_c$, respectively. The numerical results of n_s and r are calculated at horizon traversing CMB e -fold number (N_*).

| # | n_s | r | $\mathcal{P}_{\mathcal{R}}^{\text{peak}}$ | $k_{\text{peak}}/\text{Mpc}^{-1}$ | $f_{\text{PBH}}^{\text{peak}}$ | $M_{\text{PBH}}^{\text{peak}}/M_{\odot}$ |
|--------|--------|--------|---|-----------------------------------|--------------------------------|--|
| Case A | 0.9731 | 0.0419 | 0.050 | 3.52×10^6 | 0.0012 | 19.10 |
| Case B | 0.9701 | 0.0373 | 0.0423 | 5.70×10^8 | 0.0355 | 7.28×10^{-6} |
| Case C | 0.9696 | 0.0360 | 0.034 | 2.95×10^{12} | 0.9615 | 2.713×10^{-13} |
| Case D | 0.9689 | 0.0367 | 0.0312 | 4.812×10^{13} | 0.9526 | 1.023×10^{-15} |

in comparison with CMB scales, which is sufficient value to generate PBHs. Thus, in the following an estimated connection between $\mathcal{P}_{\mathcal{R}}$ at $\phi = \phi_c$ and $\mathcal{P}_{\mathcal{R}}$ at $\phi = \phi_*$ is inferred, as regards the field value at the moment of horizon traversing by pivot scale denotes by ϕ_* . Utilizing equations (23) and (31)-(34) we obtain

$$\mathcal{P}_{\mathcal{R}} \simeq \frac{\lambda e^{k\phi}}{12k^2\pi^2} \left[1 + qe^{(k+\alpha)\phi} \left(1 + \frac{\omega}{\sqrt{1 + (\frac{\phi - \phi_c}{\sigma})^2}} \right) \right], \quad (35)$$

where

$$q \equiv \frac{\lambda}{M^2}, \quad (36)$$

supposing the following proviso

$$\omega \gg 1, \quad |\phi_* - \phi_c| \gg \sigma\omega, \quad (37)$$

after all, in a rough approximation we conclude

$$\mathcal{P}_{\mathcal{R}} \Big|_{\phi=\phi_c} \simeq \omega \times \mathcal{P}_{\mathcal{R}} \Big|_{\phi=\phi_*}. \quad (38)$$

As regards $\mathcal{P}_{\mathcal{R}}$ at the moment of horizon crossing (24), for $\omega \sim \mathcal{O}(10^7)$ the acme of scalar power spectrum at $\phi = \phi_c$ could increase to order $\mathcal{O}(10^{-2})$. Taking the above approximation (38) and the mentioned provisoes (37) into account, we specify $\alpha = 40$, $q = 20$, $k = 8$, and adjust four disparate parameter Cases listed in Table I. It should be noting that, our model is delineated by a collection of eight parameters as $\{k, \alpha, M, \lambda, q, \omega, \phi_c, \sigma\}$, whereas the parameters M , q , and λ are associated together through equation (36). Table II embodies

the computed numerical results for quantities pertinent to inflation n_s , r , and the ones affiliated to PBHs formation.

As regards the duration of observable inflationary epoch thereabout 50-60 e -folds number from the time of horizon traversing via pivot scale k_* to the end of inflation, and so as to have a viable inflationary era, we adjust the e -fold number of horizon traversing N_* as 53 for Case A, 58 for Case B, and 60 for Cases C and D. The schemed results in Fig. 2 for the first slow-roll parameter illustrate that, the end of inflationary era is stipulated at the e -fold number $N_{\text{end}} = 0$ for all Cases of our model through resolving $\varepsilon = 1$. As we mentioned in the preceding section, the first slow-roll parameter ε in our NMDC setup can be approximated by equation (14), in which the presence of coupling function $\theta(\phi)$ by way of \mathcal{A} leads to bring the ε to one at $N_{\text{end}} = 0$ and terminate the inflationary era for exponential potential (34). It is obvious from equation (14) that, for $\theta(\phi) = 0$ and $\mathcal{A} = 1$ the standard slow-roll inflationary model is retrieved with $\varepsilon = \varepsilon_v = k^2/2$, which is a constant value and leads to endless inflation driven by exponential potential. In pursuance of comprehending the evolution of inflaton field versus e -folds number we need to unravel the background equations (2)-(4) exactly, utilizing the exponential potential (34) and NMDC coupling function (31)-(33). Thereafter, in Fig. 1 we exhibit the accurate status of the inflaton field ϕ and its velocity $\frac{d\phi}{dN}$ with regard to e -folds number N ($dN = -Hdt$) from N_* the horizon traversing to N_{end} the end of inflation, for the Cases A, B, C, and D by purple, green, red, and blue lines. For all Cases of this figure, There is an ephemeral smooth domain (Ultra Slow-Roll phase) continuing for about 20 e -folds in the vicinity of $\phi = \phi_c$. By reason of dominance of intensified friction during this USR phase the inflaton field rotates in a very leisurely way and the slow-roll proviso is violated, thus the sufficient time to enhance the amplitude of curvature power spectrum to around order $\mathcal{O}(10^{-2})$ can be provided. The sever decline in the velocity of the inflaton field during the USR phase is obvious from the right plots of Fig. 1 for all Cases. Hereupon, intensification of curvature power spectrum at small scale in the course of USR period is schemed in Fig. 3.

The mutation of slow-roll parameters ε and δ_ϕ with regard to the e -fold number N in the course of observable inflationary epoch $\Delta N = N_* - N_{\text{end}}$ are represented in left and right plots of Fig. 2 for all Cases of Table I. With regard to left plots of Fig. 2, the severe diminution in the value of first slow-roll parameter ε to around order $\mathcal{O}(10^{-10})$ in USR domain occurs for all Cases of our model, that can lead to intensification in the amplitude

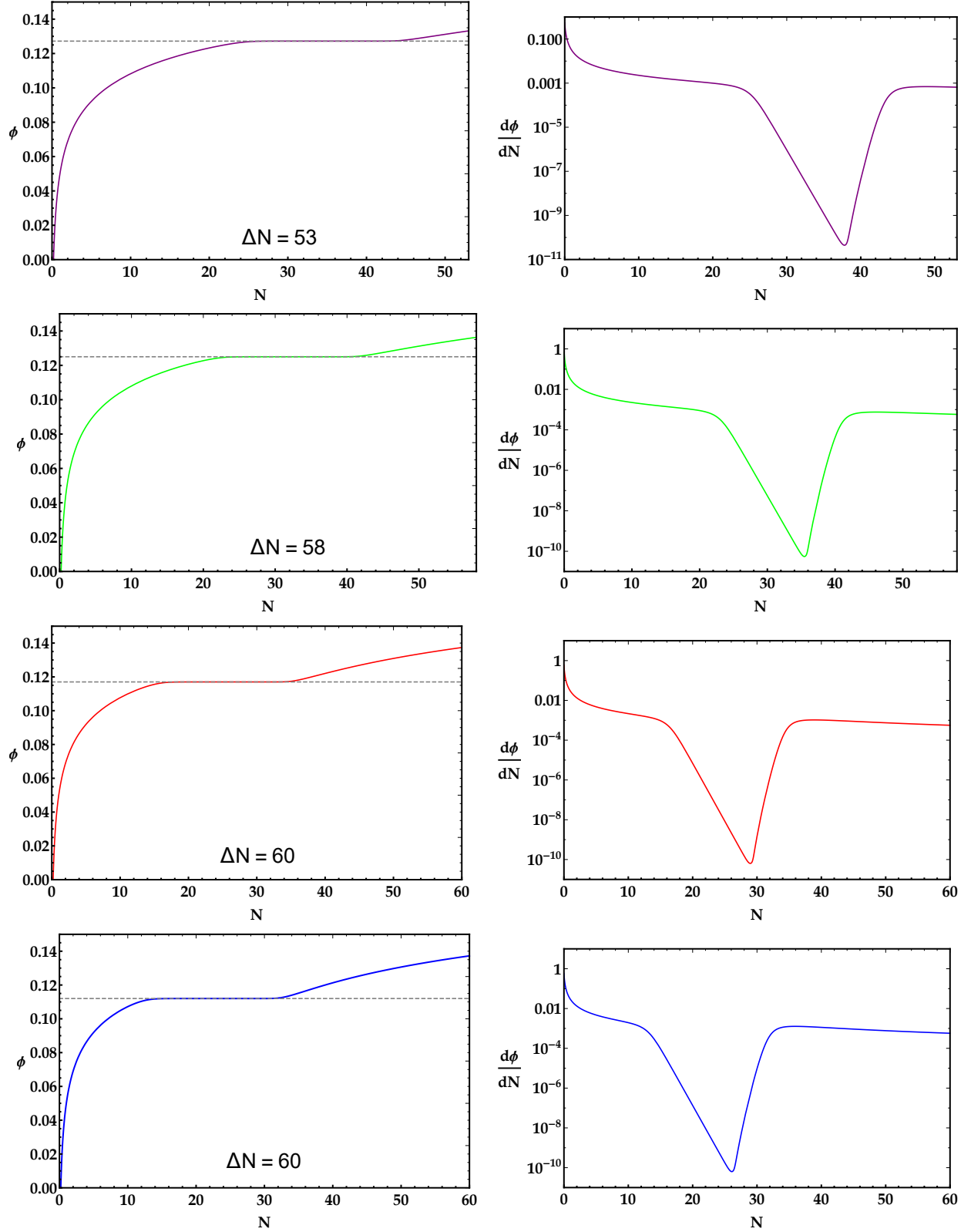


FIG. 1. (left) Variation of the scalar field ϕ , (right) the velocity of the scalar field $\frac{d\phi}{dN}$ against the e -fold number N for the Cases A, B, C, and D represented by purple, green, red, and blue lines, respectively. The acme position $\phi = \phi_c$ is represented by dashed line for all Cases in left plots, and slow-roll approximation Eqs. (11) and (13) are utilized for the incipient conditions.

of scalar power spectrum. Furthermore, from left plots of Fig. 2, it can be inferred that the mentioned slow-roll proviso is contravened via the second slow-roll parameter δ_ϕ through exceeding one in the course of USR stage momentarily. Note that it can be seen from the mutation of slow-roll parameters in Fig. 2 that, the slow-roll provisos at horizon traversing e -fold number N_* are satisfied for each Case, thereupon Eqs. (25) and (28) can be applied to compute the scalar spectral index n_s and tensor-to-scalar ratio r in our framework. The numerical computations epitomized in Table II corroborate that in view of Planck 2018 TT,TE,EE+lowE+lensing+BK14+BAO data the quantity of r for the entire Cases and n_s for the Cases B, C, and D are consistent with 68% CL, whereas n_s for Case A is consonant with 95% CL [67]. As a consequence of choosing NMDC groundwork and appropriate exponential form of coupling parameter for our model, we could rectify the observational prognostications of exponential potential.

By reason of invalidity of slow-roll approximation in USR domain, we cannot utilize Eq. (35) to compute the curvature fluctuations power spectrum in this stage owing to deriving from slow-roll approximation. Thereupon so as to attain the precise value of curvature power spectrum, the numerical evaluation of the succeeding Mukhanov-Sasaki (MS) equation is necessitated for the entire Fourier modes

$$v_k'' + \left(c_s^2 k^2 - \frac{z''}{z} \right) v_k = 0, \quad (39)$$

in which the prime denotes derivative with regard to the conformal time $\eta = \int a^{-1} dt$, and

$$v \equiv z\mathcal{R}, \quad z = a\sqrt{2Q_s}. \quad (40)$$

It is worth noting that, the mutation of curvature fluctuations \mathcal{R} in Fourier space v_k in the course of inflationary epoch from sub-horizon scales $c_s k \gg aH$ to super-horizon scales $c_s k \ll aH$ is evaluated by MS equation (39). We appoint the Fourier transformation of the Bunch-Davies vacuum state as the incipient proviso at the sub-horizon scale [72] as follows

$$v_k \rightarrow \frac{e^{-ic_s k \eta}}{\sqrt{2c_s k}}. \quad (41)$$

Subsequent to attain the numerical solutions of the MS equation (39), the accurate curvature fluctuations power spectrum for each mode v_k can be acquired as

$$\mathcal{P}_{\mathcal{R}} = \frac{k^3}{2\pi^2} \left| \frac{v_k^2}{z^2} \right|_{c_s k \ll aH}. \quad (42)$$

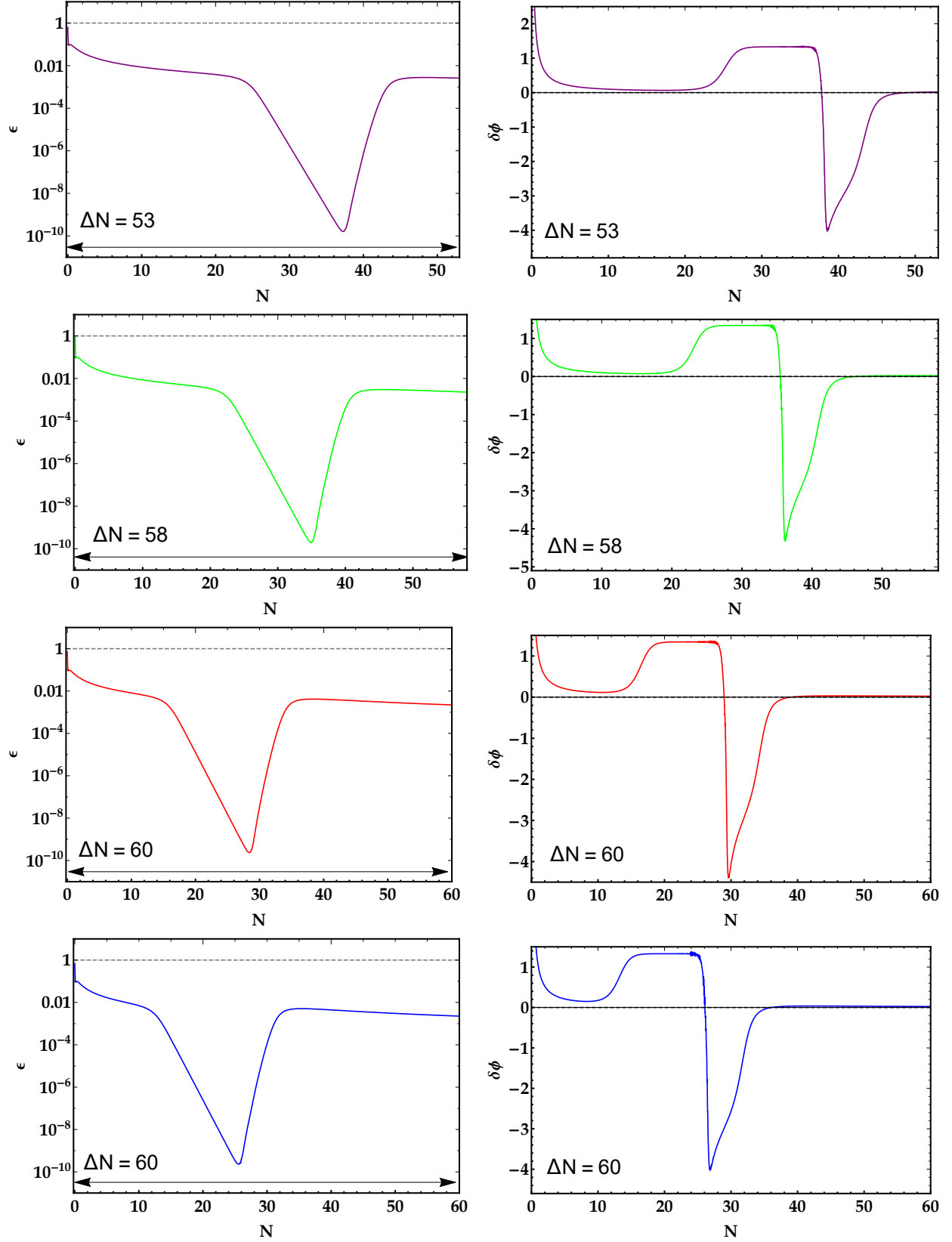


FIG. 2. Variation of (left) the first slow-roll parameter ϵ , (right) the second slow-roll parameter $\delta\phi$, with regard to the e -fold number N for the Cases A, B, C, and D represented by purple, green, red, and blue lines, respectively.

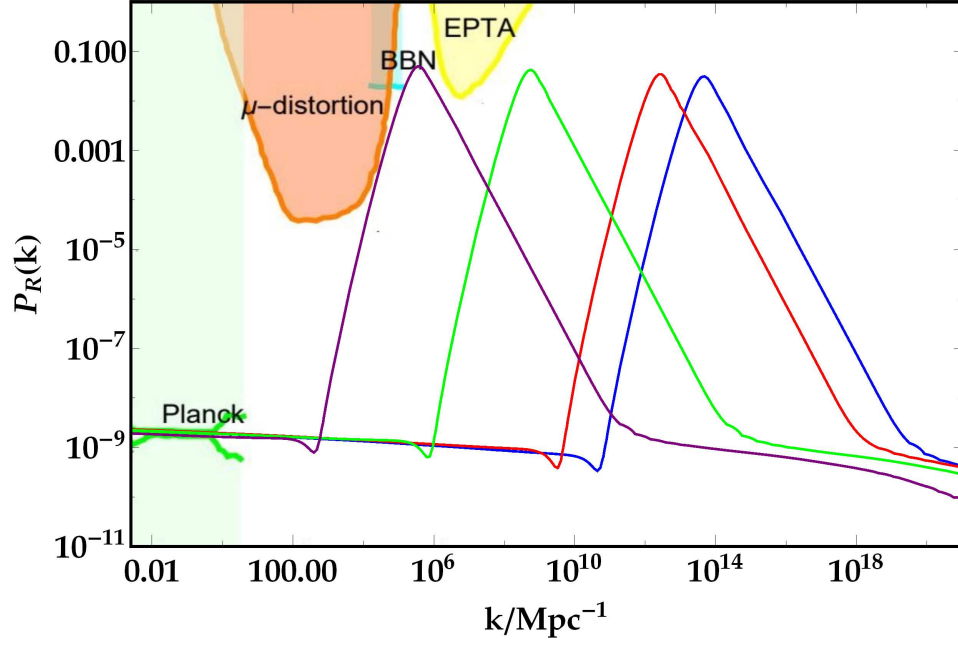


FIG. 3. The attained precise curvature fluctuations power spectrum with regard to comoving wavenumber k ensued from resolving the Mukhanov-Sasaki equation numerically. The purple, green, red and blue lines appertain to the Cases A, B, C, and D, respectively. The light-green, yellow, cyan, and orange shadowy domains depict the confinements of CMB observations [67], PTA observations [97], the effect on the ratio between neutron and proton during the big bang nucleosynthesis (BBN) [98], and the μ -distortion of CMB [99], respectively.

Table II embodies the numerical outcomes for the precise acme value of the scalar power spectrum $\mathcal{P}_{\mathcal{R}}^{\text{peak}}$, and associated comoving wavenumber k_{peak} for each Case of Table I. Moreover, in Fig. 3 the precise power spectra for the entire Cases of Table I with regard to the comoving wavenumber k , thereto the present observational confinements are delineated. In this figure the accurate $\mathcal{P}_{\mathcal{R}}$ pertinent to the Cases A, B, C, and D portrays as the purple, green, red, and blue lines, respectively. Into the bargain, it can be inferred from the Fig. 3 that, the amplitude of scalar power spectra for the entire Cases take nearly constant value around $\mathcal{O}(10^{-9})$ in the course of slow-roll inflationary era on large scales in the environs of the CMB scale ($k \sim 0.05 \text{ Mpc}^{-1}$), in consistency with the present observational data (24). Whereas, intensification in the amplitude of power spectra to order $\mathcal{O}(10^{-2})$ during the USR era on smaller scales can be perceived, which is adequate to produce detectable PBHs.

IV. GENERATION OF PRIMORDIAL BLACK HOLES

Subsequent to our preceding explications, this section is devoted to inquiry about formation of PBHs in NMDC framework emanated from sufficient multiplication of the amplitude of curvature fluctuations on small scales. Whereupon the super-horizon enhanced fluctuation modes created during the inflationary era revert to the horizon in the RD epoch, the collapse of ultra-condensed districts pertinent to these modes gives rise to generate PBHs. The mass of nascent PBHs is pertaining to the horizon mass at the time of reverting by way of

$$M_{\text{PBH}}(k) = \gamma \frac{4\pi}{H} \Big|_{c_s k = aH} \simeq M_{\odot} \left(\frac{\gamma}{0.2} \right) \left(\frac{10.75}{g_*} \right)^{\frac{1}{6}} \left(\frac{k}{1.9 \times 10^6 \text{Mpc}^{-1}} \right)^{-2}, \quad (43)$$

where γ denotes the efficiency of collapse, which is contemplated as $\gamma = (\frac{1}{\sqrt{3}})^3$ [4], and g_* signifies the efficient number of relativistic species upon thermalization in RD era, which is specified as $g_* = 106.75$ in the Standard Model of particle physics at high temperature. Utilizing the Press-Schechter theory and with the presupposition of Gaussian statistics for distribution of curvature fluctuations, the formation rate for PBHs with mass $M(k)$ is computed [106, 107] as the subsequent form

$$\beta(M) = \int_{\delta_c} \frac{d\delta}{\sqrt{2\pi\sigma^2(M)}} e^{-\frac{\delta^2}{2\sigma^2(M)}} = \frac{1}{2} \text{erfc} \left(\frac{\delta_c}{\sqrt{2\sigma^2(M)}} \right), \quad (44)$$

wherein “erfc” denotes the error function complementary, and δ_c depicts the threshold value of the density perturbations for PBHs production which is taken as $\delta_c = 0.4$ pursuant to [108, 109]. Furthermore $\sigma^2(M)$ designates the coarse-grained density contrast with the smoothing scale k , and defines as

$$\sigma_k^2 = \left(\frac{4}{9} \right)^2 \int \frac{dq}{q} W^2(q/k) (q/k)^4 \mathcal{P}_{\mathcal{R}}(q), \quad (45)$$

where $\mathcal{P}_{\mathcal{R}}$ is the curvature power spectrum, and W signifies the window function which stipulated as Gaussian window $W(x) = \exp(-x^2/2)$. In pursuance of determining the abundance of PBHs, the present fraction of density parameters related to PBHs (Ω_{PBH}) and Dark Matter (Ω_{DM}) is given as the subsequent form

$$f_{\text{PBH}}(M) \simeq \frac{\Omega_{\text{PBH}}}{\Omega_{\text{DM}}} = \frac{\beta(M)}{1.84 \times 10^{-8}} \left(\frac{\gamma}{0.2} \right)^{3/2} \left(\frac{g_*}{10.75} \right)^{-1/4} \left(\frac{0.12}{\Omega_{\text{DM}} h^2} \right) \left(\frac{M}{M_{\odot}} \right)^{-1/2}, \quad (46)$$

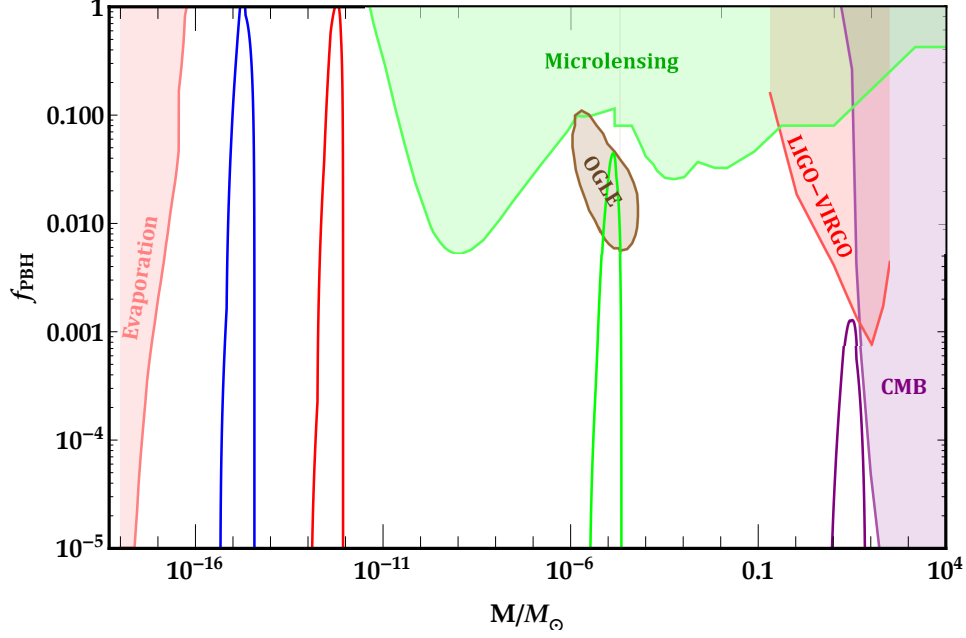


FIG. 4. The PBHs abundance f_{PBH} with regard to PBHs mass M for the Cases A, B, C, and D delineated with purple, green, red, and blue lines, respectively. The shadowy domains illustrate the recent observational constraints on the fractional abundance of PBHs. The purple area depicts the restriction on CMB from signature of spherical accretion of PBHs inside halos [110]. The border of the red shaded domain depicts the upper bound on the PBH abundance ensued from the LIGO-VIRGO event consolidation rate [111–114]. The brown shadowy domain portrays the authorized region for PBH abundance owing to the ultrashort-timescale microlensing events in the OGLE data [36]. The green shaded area allots to constraints of microlensing events from cooperation between MACHO [115], EROS [116], Kepler [117], Icarus [118], OGLE [36], and Subaru-HSC [119]. The pink shadowy region delineates the constraints related to PBHs evaporation such as extragalactic γ -ray background [120], galactic center 511 keV γ -ray line (INTEGRAL) [39], and effects on CMB spectrum [121].

wherein the current density parameter of Dark Matter $\Omega_{\text{DM}} h^2 \simeq 0.12$ is delineated by Planck 2018 data [67].

Ultimately, by settling the accurate scalar power spectrum acquired from numerical solution of Mukhanov-Sasaki equation in (45) and utilizing Eqs. (43)-(46), we could compute the PBHs abundance for the entire Cases of Table I. Table II and Fig. 4 are delineated the attained numerical and plotted upshots.

As a consequence of our finding, for parameter collection of Case A our model prognosticates PBHs with stellar-mass around $19.10M_{\odot}$ and abundance acme at $f_{\text{PBH}}^{\text{peak}} \simeq 0.0012$, which are consonant with the upper bound of the LIGO-VIRGO consolidation rate, and they can be appropriate entrant to elucidate the GWs and the LIGO-VIRGO events.

Apropos of Case B the prognosticated PBHs with earth-mass around $M_{\text{PBH}}^{\text{peak}} = 7.28 \times 10^{-6}M_{\odot}$ and abundance of $f_{\text{PBH}}^{\text{peak}} = 0.0355$, are localized in the authorized domain of the ultrashort-timescale microlensing events in OGLE data, hence this Case of PBHs could be practical to narrate microlensing events.

The parameter collections of Cases C and D of our model, give rise to foretell two PBHs mass spectra in asteroid-mass range with masses $M_{\text{PBH}}^{\text{peak}} = 2.713 \times 10^{-13}M_{\odot}$ and $M_{\text{PBH}}^{\text{peak}} = 1.023 \times 10^{-15}M_{\odot}$, and acmes of $f_{\text{PBH}}^{\text{peak}}$ at around 0.9615 and 0.9526. Ergo, they could be contemplated as desirable nominee for the entire of DM content.

It is worth noting that, recently the significant effects of quantum diffusion on curvature perturbations produced during USR, and undeniable consequences of that on PBHs formation have been studied in literatures [122–130]. In [127, 128] applying the stochastic- δN formalism in USR stage, due to the obtained exponential tail for distribution function of curvature perturbations, an increase about several orders of magnitude in the PBHs abundance in comparison with standard results has been computed. However, in [131–134] the conflicting results have been demonstrated. in [131] it has been proven that, the stochastic effects during USR domain could be neglected due to invalidity of δN formalism and separate universe approach in USR. On the other side the authors of [132] have confirmed the results of [131] about the insignificance of the stochastic effects in USR stage, but not because of the same reason. They have reproduced precisely the known leading classical donation of observable power spectrum and bispectrum, applying the stochastic δN formalism in the USR era. Subsequently in [133] it has been proven that, the concluded curvature power spectrum from stochastic inflation accurately fits, at the linear level, the numerical result computed of solving the Mukhanov-Sasaki equation, even in the USR phase. Moreover, the authors of [134] have inferred that, extra information from the stochastic approach to inflation could not be attained in comparison with traditional perturbation theory, and there are no quantum diffusion dominated regimes in SR/USR inflation or even in the transition between these eras. Ergo, it is obvious that the effects of quantum diffusion in USR stage are currently under dispute in literatures, and we did not consider that in our model.

V. PRODUCED GWS IN NMDC FRAMEWORK

Producing of induced GWs can be contemplated as another consequence of reverting the scales pertinent to enhanced amplitude of incipient curvature fluctuations to the horizon contemporaneous with generating of PBHs in RD era. The propagated GWs in the cosmos could be detected by dint of multifarious detectors if their energy spectra lie inside the sensitivity scopes of them. With this feature in mind, in this section we ponder how the induced GWs in our NMDC model with exponential form of potential and coupling parameter can be produced. It is substantiated that, with regard to the second order impressions of perturbations theory, the mutation of tensor perturbations is emanated from the first order scalar perturbations. The perturbed FRW metric utilizing the conformal Newtonian gauge can be written as the subsequent form [135]

$$ds^2 = a(\eta)^2 \left\{ -(1 + 2\Psi)d\eta^2 + \left[(1 - 2\Psi)\delta_{ij} + \frac{h_{ij}}{2} \right] dx^i dx^j \right\} , \quad (47)$$

wherein η , Ψ , and h_{ij} intimate the conformal time, the first-order scalar perturbations, and the perturbation of the second-order transverse-traceless tensor, respectively. Inasmuch as the inflaton field crumbles since the end of inflationary epoch and transforms into light particles to heat the cosmos to inaugurate the RD epoch, thus the impact of inflaton field in the course of cosmic mutation in RD era can be disregarded. Thereupon, the standard Einstein formulation can be utilized to inspect the production of induced GWs in RD era coeval with PBHs generation. In pursuance of this objective, the subsequent equation of motion is considered for the second-order tensor perturbations h_{ij} [135, 136]

$$h''_{ij} + 2\mathcal{H}h'_{ij} - \nabla^2 h_{ij} = -4\mathcal{T}_{ij}^{lm} S_{lm} , \quad (48)$$

in which $\mathcal{H} \equiv a'/a$ and \mathcal{T}_{ij}^{lm} , symbolize the conformal Hubble parameter and the transverse-traceless projection operator. The GW origin term S_{ij} is contemplated as

$$S_{ij} = 4\Psi\partial_i\partial_j\Psi + 2\partial_i\Psi\partial_j\Psi - \frac{1}{\mathcal{H}^2}\partial_i(\mathcal{H}\Psi + \Psi')\partial_j(\mathcal{H}\Psi + \Psi') . \quad (49)$$

In the following the scalar metric perturbations Ψ in the Fourier space in the course of RD era is calculated by [136] as

$$\Psi_k(\eta) = \psi_k \frac{9}{(k\eta)^2} \left(\frac{\sin(k\eta/\sqrt{3})}{k\eta/\sqrt{3}} - \cos(k\eta/\sqrt{3}) \right) , \quad (50)$$

wherein k signifies the comoving wavenumber. Furthermore the incipient perturbations ψ_k is affiliated to the curvature fluctuations power spectrum by dint of the following two-pointed correlation function

$$\langle \psi_{\mathbf{k}} \psi_{\tilde{\mathbf{k}}} \rangle = \frac{2\pi^2}{k^3} \left(\frac{4}{9} \mathcal{P}_{\mathcal{R}}(k) \right) \delta(\mathbf{k} + \tilde{\mathbf{k}}) . \quad (51)$$

In the end, the following equation for energy density of induced GWs in the course of RD era is attained by [79]

$$\begin{aligned} \Omega_{\text{GW}}(\eta_c, k) = & \frac{1}{12} \int_0^\infty dv \int_{|1-v|}^{|1+v|} du \left(\frac{4v^2 - (1+v^2-u^2)^2}{4uv} \right)^2 \mathcal{P}_{\mathcal{R}}(ku) \mathcal{P}_{\mathcal{R}}(kv) \left(\frac{3}{4u^3v^3} \right)^2 (u^2 + v^2 - 3)^2 \\ & \times \left\{ \left[-4uv + (u^2 + v^2 - 3) \ln \left| \frac{3-(u+v)^2}{3-(u-v)^2} \right| \right]^2 + \pi^2 (u^2 + v^2 - 3)^2 \Theta(v + u - \sqrt{3}) \right\} , \end{aligned} \quad (52)$$

in which Θ denotes the Heaviside theta function, and η_c designates the time of ceasing the growth of Ω_{GW} . By way of the subsequent equation, the present value of the induced GWs energy spectra is affiliated to the energy spectra at η_c [97]

$$\Omega_{\text{GW}_0} h^2 = 0.83 \left(\frac{g_*}{10.75} \right)^{-1/3} \Omega_{\text{r}_0} h^2 \Omega_{\text{GW}}(\eta_c, k) , \quad (53)$$

in which the present value of radiation density parameter is indicated by $\Omega_{\text{r}_0} h^2 \simeq 4.2 \times 10^{-5}$, and $g_* \simeq 106.75$ signifies the effective degrees of freedom in the energy density at η_c . Moreover frequency is related to wavenumber through the following equation

$$f = 1.546 \times 10^{-15} \left(\frac{k}{\text{Mpc}^{-1}} \right) \text{Hz} . \quad (54)$$

In follow up our study, we utilize the accurate scalar power spectrum deduced from numerical solution of the MS equation beside Eqs. (52)-(54), and could acquire the present energy spectra of scalar induced GWs associated with PBHs for the entire Cases of Table I. The diagram of our foretold upshots beside the susceptibility curves of varietal GWs observatories are depicted in Fig. 5. It is worth noting that, rectitude of our prognosticated upshots can be verified in view of these GWs observatories which are composed of European PTA (EPTA) [137–140], the Square Kilometer Array (SKA) [141], Advanced Laser Interferometer

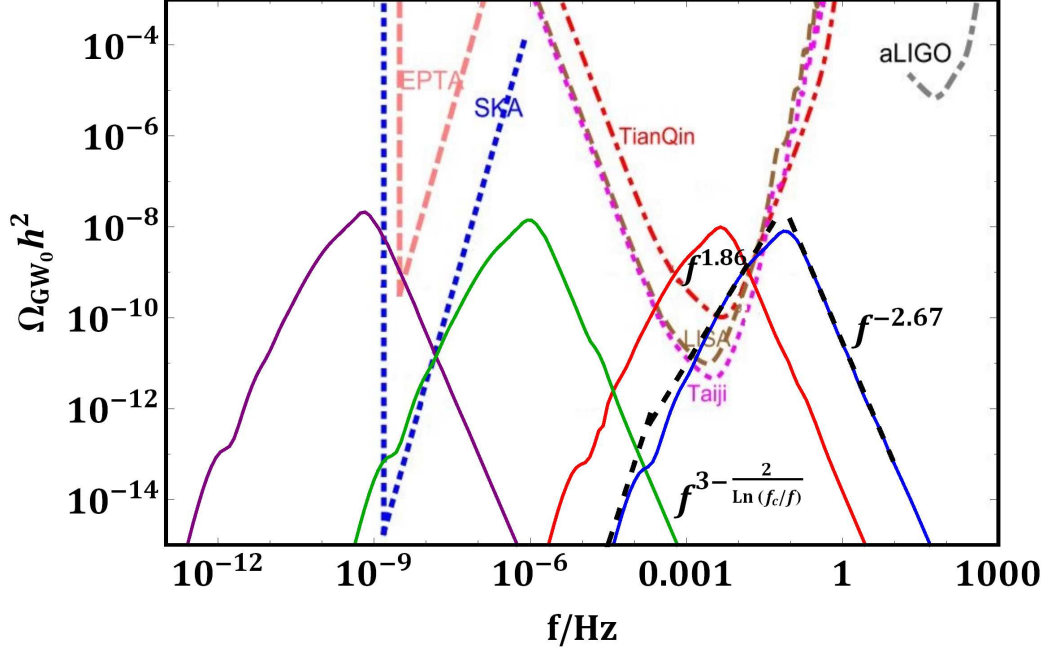


FIG. 5. The procured spectra of present induced GWs energy density parameter Ω_{GW_0} with regard to frequency pertinent to the Cases A (purple solid line), B (green solid line), C (red solid line), and D (blue solid line) of Table I. The power-law behavior of Ω_{GW_0} is depicted by black dashed line for the Case D.

Gravitational Wave Observatory (aLIGO) [142, 143], Laser Interferometer Space Antenna (LISA) [144, 145], TaiJi [146], and TianQin [147].

It is obvious from Fig. 5 that, the acmes of spectra of Ω_{GW_0} prognosticated from our setup, for the Cases A (purple line), B (green line), C (red line), and D (blue line) have located at disparate frequencies with approximately alike altitude of order 10^{-8} . For the Cases A and B appertain to stellar and earth mass PBHs, the acmes of spectra of Ω_{GW_0} have localized at frequencies around $f_c \sim 10^{-10}\text{Hz}$ and $f_c \sim 10^{-7}\text{Hz}$ respectively, which lie inside the susceptibility scope of the SKA observatory. Apropos of the Cases C and D pertinent to asteroid mass PBHs, the acmes of Ω_{GW_0} spectra settle in mHz and cHz frequency zone which could be traced by LISA, TaiJi, and TianQin observatories. Inasmuch as, the prognosticated spectra of Ω_{GW_0} for the entire Cases of our model could cross the susceptibility curves of disparate GWs observatories, the legitimacy of this model could be appraised by way of the broadcasted data of these observatories in future.

After all we scrutinize the slope of spectra of Ω_{GW_0} at the disparate frequency zones in the environs of the acme position. Newly, it has been corroborated that in the vicinity of acme

position, the current density parameter spectra of induced GWs have a power-law behaviour with regard to frequency as $\Omega_{\text{GW}_0}(f) \sim f^n$ [58, 148, 149]. In Fig. 5, the approximate slope of the spectrum of Ω_{GW_0} are mapped with black dashed lines in three ranges of frequency for the Case D. For this Case we have computed the frequency of acme as $f_c = 0.0744\text{Hz}$, and appraise the power index of power-law function $n = 1.86$ for $f < f_c$, $n = -2.67$ for $f > f_c$, and moreover a log-reliant form as $n = 3 - 2/\ln(f_c/f)$ for the infrared region $f \ll f_c$, which is consonant with the analytic sequels procured in [150, 151].

VI. CONCLUSIONS

In this work, the PBHs generation in the inflationary model pertinent to the Horndenski theory with nonminimal coupling between the field derivative and the Einstein tensor expounded by action (1) is verified. The enhancement of friction gravitationally emanated from nonminimal field derivative coupling to gravity setup making the inflaton slow down and gives rise to a transient stage in the dynamics of scalar field namely ultra slow-roll inflationary era. With this trait in mind, whereas in standard framework of inflation the exponential potential drives an endless inflationary epoch [78] and, as regards the inconsistency of the prognostications of this form of potential at CMB scales with Planck 2018 data [67, 78], we contemplated it in NMDC setup and try to amend its foretold outcomes.

By considering exponential potential for our model beside defining coupling parameter as two-parted exponential function of inflaton field (31)-(33), and thence fine-tuning of the four parameter collections (A, B, C, and D) depicted in Table I, we were able to slow down the inflaton velocity adequately to produce PBHs in an ultra slow-roll phase on small scales. Another consequence of these choices is that the observational results of the model were obtained in accordance with Planck 2018 data on CMB scales.

Furthermore, we delineated mutation diagram of inflaton field ϕ , the first and second slow-roll parameters (ε and δ_ϕ) in terms of e -fold number N in Figs. 1 and 2 by way of accurate solving of the background equations (2)-(4). As regards the mutation diagram of slow-roll parameters in Fig. 2 it can be inferred that, in the course of USR stage ε adheres to the slow-roll provisos ($\varepsilon \ll 1$) but δ_ϕ contravenes that ($|\delta_\phi| \gtrsim 1$). Hence, we calculated the accurate curvature fluctuations power spectra appertain to the entire Cases of Table I by numerical solving of the Mukhanov-Sasaki equation. The numerical upshots epitomized

in Table II and schemed diagram in Fig. 3 illustrate that, the attained accurate power spectra have approximately constant values in consistency with the Planck 2018 data on CMB scales, whereas on smaller scales they have acmes with adequate altitude to produce detectable PBHs.

Regarding the obtained numerical results for n_s and r enumerated in Table II, we can see that in view of Planck 2018 TT,TE,EE+lowE+lensing+BK14+BAO data the quantity of r for the entire Cases and n_s for the Cases B, C, and D are consonant with 68% CL, whereas n_s for the Case A is consonant with 95% CL [67]. As a consequence of choosing NMDC groundwork and appropriate exponential form of coupling parameter for our model, we could rectify the observational prognostications of exponential potential.

At length by utilizing the accurate scalar power spectrum acquired from numerical solution of Mukhanov-Sasaki equation and Press-Schechter formulation, we could compute the PBHs abundance for the entire Cases of Table I. Prognosticated PBHs for the Case A with stellar-mass around $19.1 M_\odot$ and abundance acme at $f_{\text{PBH}}^{\text{peak}} \simeq 0.0012$ could be appropriate to explicate the GWs and the LIGO-VIRGO events. Obtained PBHs for the Case B with earth-mass around $M_{\text{PBH}}^{\text{peak}} = 7.28 \times 10^{-6} M_\odot$ and abundance of $f_{\text{PBH}}^{\text{peak}} = 0.0355$ could be practical to narrate microlensing events. Moreover foretold PBHs for the Cases C and D with masses $M_{\text{PBH}}^{\text{peak}} = 2.713 \times 10^{-13} M_\odot$ and $M_{\text{PBH}}^{\text{peak}} = 1.023 \times 10^{-15} M_\odot$, and acmes of $f_{\text{PBH}}^{\text{peak}}$ at around 0.9615 and 0.9526 could be contemplated as desirable nominee for the entire of DM content (see Table II and Fig. 4).

At last, we investigated production of the induced GWs coeval with PBHs formation and computed the current spectra of Ω_{GW_0} for the entire Cases of our model. It is inferred from our computation that, all Cases have located at disparate frequencies with approximately alike altitude of order 10^{-8} (see Fig. 5). For the Cases A and B appertain to stellar and earth mass PBHs, the acmes of Ω_{GW_0} spectra have localized at frequencies around $f_c \sim 10^{-10}\text{Hz}$ and $f_c \sim 10^{-7}\text{Hz}$ respectively, which lie inside the susceptibility scope of the SKA observatory. Apropos of the Cases C and D pertinent to asteroid mass PBHs, the acmes of Ω_{GW_0} spectra settle in mHz and cHz frequency zone which could be traced by LISA, TaiJi, and TianQin observatories. Ergo the legitimacy of our model could be appraised by way of the broadcasted data of these observatories in future.

After all we checked the power-law behaviour of the slope of spectra of Ω_{GW_0} at the disparate frequency zones in the environs of the acme position with regard to frequency as

$\Omega_{\text{GW}_0}(f) \sim f^n$ [58, 148, 149], and we appraised the power index of power-law function $n = 1.86$ for $f < f_c$, $n = -2.67$ for $f > f_c$, and moreover a log-reliant form as $n = 3 - 2/\ln(f_c/f)$ for the infrared region $f \ll f_c$, which is consonant with the analytic sequels of [150, 151].

-
- [1] Ya. B. Zel'dovich and I. D. Novikov, *Sov. Astron.* **10**, 602 (1967).
 - [2] S. Hawking, *Mon. Not. R. Astron. Soc.* **152**, 75 (1971).
 - [3] B. J. Carr and S.W. Hawking, *Mon. Not. R. Astron. Soc.* **168**, 399 (1974).
 - [4] B. J. Carr, *Astrophys. J.* **201**, 1 (1975).
 - [5] K. Garrett and G. Duda, *Adv. Astron.* **2011**, 968283 (2011).
 - [6] B. P. Abbott et al. (LIGO Scientific Collaboration and Virgo Collaboration), *Phys. Rev. Lett.* **116**, 061102 (2016).
 - [7] B. P. Abbott et al. (LIGO Scientific Collaboration and Virgo Collaboration), *Phys. Rev. Lett.* **116**, 241103 (2016).
 - [8] B. P. Abbott et al. (LIGO Scientific Collaboration and Virgo Collaboration), *Phys. Rev. Lett.* **116**, 221101 (2017).
 - [9] B. P. Abbott et al. (LIGO Scientific Collaboration and Virgo Collaboration), *Astrophys. J.* **851**, L35 (2017).
 - [10] B. P. Abbott et al. (LIGO Scientific Collaboration and Virgo Collaboration), *Phys. Rev. Lett.* **119**, 141101 (2017).
 - [11] P. Ivanov, P. Naselsky and I. Novikov, *Phys. Rev. D* **50**, 7173-7178 (1994).
 - [12] P. H. Frampton, M. Kawasaki, F. Takahashi and T. T. Yanagida, *JCAP* **04**, 023 (2010).
 - [13] K. Inomata, M. Kawasaki, K. Mukaida, Y. Tada and T. T. Yanagida, *Phys. Rev. D* **96** no.4, 043504 (2017).
 - [14] B. Carr and F. Kuhnel, *Ann. Rev. Nucl. Part. Sci.* **70**, 355-394 (2020).
 - [15] S. Bird, I. Cholis, J. B. Muñoz, Y. Ali-Haïmoud, M. Kamionkowski, E. D. Kovetz, A. Raccanelli, and A. G. Riess, *Phys. Rev. Lett.* **116**, 201301 (2016).
 - [16] S. Clesse and J. García-Bellido, *Phys. Dark Universe* **15**, 142 (2017).
 - [17] M. Sasaki, T. Suyama, T. Tanaka, and S. Yokoyama, *Phys. Rev. Lett.* **117**, 061101 (2016).
 - [18] B. Carr, F. Kuhnel, and M. Sandstad, *Phys. Rev. D* **94**, 083504 (2016).
 - [19] K. M. Belotsky et al, *Mod. Phys. Lett. A*, **29**, 1440005 (2014).

- [20] K. M. Belotsky et al, Eur. Phys. J. C, **79**, 246 (2019).
- [21] M. Solbi and K. Karami, Eur. Phys. J. C **81**, 884 (2021).
- [22] M. Solbi and K. Karami, JCAP, **08**, 056 (2021).
- [23] Z. Teimoori, K. Rezazadeh, M. A. Rasheed, K. Karami, JCAP, **10**, 018 (2021).
- [24] K. Rezazadeh, Z. Teimoori, K. Karami, arXiv:2110.01482.
- [25] M. R. Gangopadhyay, J. C. Jain, D. Sharma, Yogesh, arXiv:2108.13839.
- [26] G. Domènech, Universe **7** 11, 398 (2021).
- [27] G. Domènech, Int. J. Mod. Phys. D **29** 03, 2050028 (2020).
- [28] G. Domènech, and M. Sasaki, Phys. Rev. D **103**, 063531 (2021).
- [29] R. Kimura, T. Suyama, M. Yamaguchi, Y. Zhang, JCAP, **04**, 031 (2021).
- [30] S. Kawai and J. Kim, Phys. Rev. D **104**, no.4, 043525 (2021).
- [31] S. Kawai and J. Kim, Phys. Rev. D **104**, no.8, 083545 (2021).
- [32] J. Lin, S. Gao, Y. Gong, Y. Lu, Z. Wang, F. Zhang, arXiv:2111.01362.
- [33] F. Zhang, J. Lin, Y. Lu, Phys. Rev. D **104**, 063515 (2021).
- [34] J. Lin, Q. Gao, Y. Gong, Y. Lu, C. Zhang, F. Zhang, Phys. Rev. D **101**, 103515 (2020).
- [35] Y. Lu, A. Ali, Y. Gong, J. Lin, F. Zhang, Phys. Rev. D **102**, 083503 (2020).
- [36] H. Niikura, M. Takada, S. Yokoyama, T. Sumi, and S. Masaki, Phys. Rev. D **99**, 083503 (2019).
- [37] A. Katz, J. Kopp, S. Sibiryakov, and W. Xue, JCAP, **12**, 005 (2018).
- [38] H. Niikura et al., Nat. Astron. **3**, 524 (2019).
- [39] R. Laha, Phys. Rev. Lett. **123**, 251101, (2019).
- [40] M. Yu. Khlopov, Res. Astron. Astrophys. **10**, 495 (2010).
- [41] Y. F. Cai, X. Tong, D. G. Wang, and S. F. Yan, Phys. Rev. Lett. **121**, 081306 (2018).
- [42] G. Ballesteros, J. Rey, M. Taoso, A. Urbano, JCAP **07**, 025 (2020).
- [43] A. Y. Kamenshchik, A. Tronconi, T. Vardanyan, and G. Venturi, Phys. Lett. B **791**, 201 (2019).
- [44] I. Dalianis, A. Kehagias, and G. Tringas, JCAP **01**, 037 (2019).
- [45] R. Mahbub, Phys. Rev. D **101**, 023533 (2020).
- [46] S. S. Mishra and V. Sahni, JCAP **04**, 007 (2020).
- [47] J. Fumagalli, S. Renaux-Petel, J. W. Ronayne, and L. T. Witkowski, arXiv:2004.08369.
- [48] M. Braglia, D. K. Hazra, F. Finelli, G. F. Smoot, L. Sriramkumar, A. A. Starobinsky, JCAP

- 08** 001 (2020).
- [49] M. Braglia, X. Chen, D. K. Hazra, JCAP **03** 005 (2021).
 - [50] I. Dalianis, G. P. Kodaxis, I. D. Stamou, N. Tetradis, and A. Tsigkas-Kouvelis, Phys. Rev. D **104**, 103510 (2021).
 - [51] J. Garcia-Bellido, E. R. Morales, Phys. Dark Univ **18** 47-54 (2017).
 - [52] C. Germani, T. Prokopec, Phys. Dark Univ **18** 6-10 (2017).
 - [53] G. Ballesteros, M. Taoso, Phys. Rev. D **97**, 023501 (2018).
 - [54] J. Liu, Z. K. Guo, and R. G. Cai, Phys. Rev. D **101**, 023513 (2020).
 - [55] C. Fu, P. Wu, H. Yu, Phys. Rev. D **100**, 063532, (2019)
 - [56] Z. Teimoori, K. Rezazadeh, K. Karami, Astrophys. J. **915**, 118 (2021).
 - [57] S. Heydari, K. Karami, Eur. Phys. J. C **82**, 83 (2022).
 - [58] C. Fu, P. Wu, H. Yu, Phys. Rev. D **101**, 023529, (2020).
 - [59] I. Dalianis, S. Karydas, and E. Papantonopoulos, JCAP **06**, 040 (2020).
 - [60] B. Dasgupta, R. Laha, and A. Ray, Phys. Rev. Lett. **125**, 101101 (2020).
 - [61] S. Pi, Y. Zhang, M. Sasaki and Q. G. Huang JCAP **05**, 042 (2018).
 - [62] H. Motohashi and W. Hu, Phys. Rev. D **96**, 063503 (2017).
 - [63] J. Garcia-Bellido, M. Peloso, C. Unal, 2017, JCAP, **09**, 013 (2017)
 - [64] A. Barnacka, J. F. Glicenstein, and R. Moderski, Phys. Rev. D **86**, 043001 (2012).
 - [65] P. W. Graham, S. Rajendran, and J. Varela, Phys. Rev. D **92**, 063007 (2015).
 - [66] P. Montero-Camacho et al. JCAP **08**, 031 (2019).
 - [67] Y. Akrami et al. (Planck Collaboration), Astron. Astrophys. **641**, A10 (2020).
 - [68] C. Germani and A. Kehagias, Phys. Rev. Lett. **105**, 011302 (2010).
 - [69] A. De Felice, S. Tsujikawa, Phys. Rev. D **84**, 083504 (2011).
 - [70] S. Tsujikawa, Phys. Rev. D **85**, 083518 (2012).
 - [71] S. Tsujikawa, J. Ohashi, S. Kuroyanagi, and A. De Felice, Phys. Rev. D **88**, 023529 (2013).
 - [72] A. De Felice, S. Tsujikawa, JCAP **03**, 030 (2013).
 - [73] G. W. Horndeski, IJTP, **10**, 363, (1974).
 - [74] M. Ostrogradski, Mem. Ac. St. Petersburg, **6**, 385, (1850).
 - [75] T. J. Chen, M. Fasiello, E. A. Lim, and A. J. Tolley, JCAP **02**, 042 (2013).
 - [76] C. de Rham, and A. Matas, JCAP **06**, 041 (2016).
 - [77] D. Langlois, and K. Noui, JCAP **02**, 034 (2016).

- [78] Z. Teimoori, K. Karami, Nucl. Phys. B **21**, 25 (2017).
- [79] K. Kohri and T. Terada, Phys. Rev. D **97**, 123532 (2018).
- [80] R. G. Cai, S. Pi, and M. Sasaki, Phys. Rev. Lett. **122**, 201101 (2019).
- [81] R. G. Cai, S. Pi, S. J. Wang, and X. Y. Yang, JCAP **05**, 013 (2019).
- [82] N. Bartolo, V. De Luca, G. Franciolini, A. Lewis, M. Peloso, and A. Riotto, Phys. Rev. Lett. **122**, 211301 (2019).
- [83] N. Bartolo, V. De Luca, G. Franciolini, M. Peloso, D. Racco, and A. Riotto, Phys. Rev. D **99**, 103521 (2019).
- [84] S. Wang, T. Terada, and K. Kohri, Phys. Rev. D **99**, 103531 (2019).
- [85] Y. F. Cai, C. Chen, X. Tong, D. G. Wang, and S. F. Yan, Phys. Rev. D **100**, 043518 (2019).
- [86] W. T. Xu, J. Liu, T. J. Gao, and Z. K. Guo, Phys. Rev. D **101**, 023505 (2020).
- [87] Y. Lu, Y. Gong, Z. Yi, and F. Zhang, JCAP **12**, 031 (2019).
- [88] F. Hajkarim and J. Schaffner-Bielich, Phys. Rev. D **101**, 043522 (2020).
- [89] J. Fumagalli, S. Renaux-Petel, and L. T. Witkowski, arXiv:2012.02761 (2020).
- [90] H. Di and Y. Gong, JCAP **07**, 007 (2018).
- [91] R. Namba, M. Peloso, M. Shiraishi, L. Sorbo, C. Unal, JCAP, **01**, 041, (2016).
- [92] M. Kawasaki, A. Kusenko, Y. Tada, T. T. Yanagida, Phys. Rev. D **94**, 083523 (2016).
- [93] K. Kannike, L. Marzola, M. Raidal, and H. Veermäe, JCAP **09** 020 (2017).
- [94] J. Garcia-Bellido, A. D. Linde, and D. Wands, Phys. Rev. D **54**, 6040 (1996).
- [95] S. Clesse and J. Garcia-Bellido, Phys. Rev. D **92**, 023524 (2015).
- [96] L. N. Granda, D. F. Jimenez, W. Cardona, Astropart. Phys. **121**, 102459 (2020).
- [97] K. Inomata and T. Nakama, Phys. Rev. D **99**, 043511 (2019).
- [98] K. Inomata, M. Kawasaki, and Y. Tada, Phys. Rev. D **94**, 043527 (2016).
- [99] D. J. Fixsen, E. S. Cheng, J. M. Gales, J. C. Mather, R. A. Shafer, and E. L. Wright, Astrophys. J. **473**, 576 (1996).
- [100] R. Allahverdi, R. Brandenberger, F.-Y. Cyr-Racine, and A. Mazumdar, Annu. Rev. Nucl. Part. Sci. **60**, 27 (2010).
- [101] L. F. Abbott, E. Farhi, and M. B. Wise, Phys. Lett. **117B**, 29 (1982).
- [102] A. D. Dolgov and A. D. Linde, Phys. Lett. **116B**, 329 (1982).
- [103] A. J. Albrecht, P. J. Steinhardt, M. S. Turner, and F. Wilczek, Phys. Rev. Lett. **48**, 1437 (1982).

- [104] A. R. Liddle and S. M. Leach, Phys. Rev. D **68**, 103503 (2003).
- [105] J. Martin and C. Ringeval, Phys. Rev. D **82**, 023511 (2010).
- [106] Y. Tada, S. Yokoyama, Phys. Rev. D **100**, 023537 (2019).
- [107] S. Young, C. T. Byrnes, M. Sasaki, JCAP **07** 045 (2014).
- [108] I. Musco, J. C. Miller, Class. Quant. Grav. **30**, 145009 (2013).
- [109] T. Harada, C.-M. Yoo, K. Kohri, Phys. Rev. D **88**, 084051 (2013).
- [110] P. D. Serpico, V. Poulin, D. Inman, and K. Kohri, Phys. Rev. Res. **2**, 023204 (2020).
- [111] B. J. Kavanagh, D. Gaggero, and G. Bertone, Phys. Rev. D **98**, 023536 (2018).
- [112] B. P. Abbott, R. Abbott, T. D. Abbott, S. Abbott, F. Abraham, K. Acernese, et al. Phys. Rev. Lett. **123**, 161102 (2019).
- [113] Z.-C. Chen, Q.-G. Huang, JCAP **20**, 039 (2020).
- [114] C. Boehm, A. Kobakhidze, C. A. J. O'hare, Z. S. C. Picker, M. Sakellariadou, JCAP **03**, 078 (2021).
- [115] C. Alcock, R. A. Allsman, D. R. Alves, T. S. Axelrod, A. C. Becker, D. P. Bennett, et al. Astrophys. J. Lett. **550**, L169 (2001).
- [116] P. Tisserand, L. Le Guillou, C. Afonso, J. N. Albert, J. Andersen, E. Ansari, et al. Astron. Astrophys. **469**, 387–404 (2007).
- [117] K. Griest, A. M. Cieplak, M. J. Lehner, Astrophys. J. **786**, 158 (2014).
- [118] M. Oguri, J. M. Diego, N. Kaiser, P. L. Kelly, T. Broadhurst, Phys. Rev. D **97**, 023518 (2018).
- [119] D. Croon, D. McKeen, N. Raj, Z. Wang, Phys. Rev. D **102**, 083021 (2020).
- [120] B. J. Carr, K. Kohri, Y. Sendouda, and J. Yokoyama, Phys. Rev. D **81**, 104019 (2010).
- [121] S. Clark, B. Dutta, Y. Gao, L. E. Strigari, S. Watson, Phys. Rev. D **95**, 083006 (2017).
- [122] J. M. Ezquiaga, J. Garcia-Bellido, and V. Vennin, JCAP **03**, 029 (2020).
- [123] C. Pattison, V. Vennin, H. Assadullahi, and D. Wands, JCAP **10**, 046 (2017).
- [124] M. Biagetti, G. Franciolini, A. Kehagias and A. Riotto, JCAP **07**, 032 (2018).
- [125] G. Ballesteros, J. Rey, M. Taoso, and A. Urbano, JCAP **08**, 043 (2020).
- [126] C. Pattison, V. Vennin, D. Wands, and H. Assadullahi, JCAP **04**, 080 (2021).
- [127] D. G. Figueroa, S. Raatikainen, S. Rasanen, E. Tomberg, arXiv:2111.07437.
- [128] D. G. Figueroa, S. Raatikainen, S. Rasanen, and E. Tomberg, Phys. Rev. Lett. **127**, 101302 (2021).

- [129] A. De and R. Mahbub, Phys. Rev. D **102**, 123509 (2020).
- [130] J. M. Ezquiaga and J. Garcia-Bellido, JCAP **08**, 018 (2018).
- [131] D. Cruces, C. Germani, and T. Prokopec, JCAP **03**, 048 (2019).
- [132] H. Firouzjahi, A. Nassiri-Rada, and M. Noorbala, JCAP **01**, 040 (2019).
- [133] G. Ballesteros, J. Rey, M. Taosoc, A. Urbano, JCAP**08**, 043 (2020).
- [134] D.Cruces, and C. Germani, Phys. Rev. D **105**, 023533 (2022).
- [135] K. N. Ananda, C. Clarkson, and D. Wands, Phys. Rev. D **75**, 123518 (2007).
- [136] D. Baumann, P. J. Steinhardt, K. Takahashi and K. Ichiki, Phys. Rev. D **76**, 084019 (2007).
- [137] R. D. Ferdman et al., Class. Quant. Grav. **27**, 084014 (2010).
- [138] G. Hobbs et al., Class. Quant. Grav. **27**, 084013 (2010).
- [139] M. A. McLaughlin, Class. Quant. Grav. **30**, 224008 (2013).
- [140] G. Hobbs, Class. Quant. Grav. **30**, 224007 (2013).
- [141] C. J. Moore, R. H. Cole, and C. P. L. Berry, Class. Quant. Grav. **32**, 015014 (2015).
- [142] G. M. Harry (LIGO Scientific Collaboration), Class. Quant. Grav. **27**, 084006 (2010).
- [143] J. Aasi et al. (LIGO Scientific Collaboration), Class. Quant. Grav. **32**, 074001 (2015).
- [144] P. Amaro-Seoane et al. (LISA Collaboration), arXiv:1702.00786.
- [145] K. Danzmann, Class. Quant. Grav. **14**, 1399 (1997).
- [146] W.-R. Hu and Y.-L. Wu, Natl. Sci. Rev. **4**, 685 (2017).
- [147] J. Luo et al. (TianQin Collaboration), Class. Quant. Grav. **33**, 035010 (2016).
- [148] W.-T. Xu, J. Liu, T.-J. Gao, and Z.-K. Guo, Phys. Rev. D **101**, 023505 (2020).
- [149] S. Kuroyanagi, T. Chiba, and T. Takahashi, JCAP **11**, 038 (2018).
- [150] C. Yuan, Z. C. Chen, and Q. G. Huang, Phys. Rev. D **101**, 043019 (2020).
- [151] R-G. Cai, S. Pi, and M. Sasaki, Phys. Rev. D **102**, 083528 (2020).